Colloid and Polymer Science (2023) 301:879–891
https://doi.org/10.1007/s00396-023-05103-3

ORIGINAL CONTRIBUTION

Fabrication of chitosan functionalized dual stimuli-responsive injectable nanogel to control delivery of doxorubicin

Danyang Li[1] · Wenshuang Xu[1] · Hui Liu[1]

Received: 9 February 2023 / Revised: 27 March 2023 / Accepted: 29 March 2023 / Published online: 17 April 2023

Abstract

Stimuli-responsive hydrogel could respond rapidly to environmental changes, whereas the limitation of gel scale usually led to a single route of drug delivery and restricted application. Herein, a pH and temperature dual responsive nanogel CS/P(MAA-co-NIPAM) was successfully prepared by radical polymerization. The change of both turbidity and hydration diameter at different conditions indicated that the nanogel possessed obvious pH and temperature sensitive properties. Specifically, the hydration diameters of the nanogel were 234 nm at T = 20 °C and 145 nm at T = 45 °C. The schematic flowable characteristic by injection experiment indicated that CS/P(MAA-co-NIPAM) might have the potential application possibility of injectable drug delivery. In addition, with doxorubicin as the model drug, the drug loading efficiency of the nanogel was 84.00% and the maximum release efficiency reached 66.30% at pH = 2.0 & T = 20 °C. The nanogel was able to realize drug delivery process in physiological environment according to in-vitro controlled releasing experiments.

Keywords Chitosan · Injectable nanogel · Dual stimuli-responsive · Drug delivery

Introduction

Nanogels were cross-linked polymeric particles with three-dimensional structure, which usually had strong stability, considerable water content, good biocompatibility, and high specific surface area [1–3]. Owing to the dual characteristics of nanocarriers [4] and hydrogels, nanogels could not only exhibit excellent loading capability and chemical stability of nanocarriers, but also possess swelling and stimulation responsive properties similar to hydrogels [5–7]. Their nanoscale provided the possibility of deep tissue diagnosis and treatment as well as multiple routes of drug delivery compared with traditional hydrogels, hence nanogels had certain application prospects and research value in the biomedical field [8–10]. Azadia et al. [11] prepared nanogels loaded with methotrexate (MTX) using chitosan (CS) and sodium tripolyphosphate, and the results showed that the nanogels significantly increased the concentration of MTX at the patient site. Rudmianeh et al. [12] developed pH-responsive nanogels by adding sodium polyanionic alginate to CS and proved that CS could effectively enhance pH-sensitive properties of the nanogels. Although many research works on nanogels had been reported, the high price of prepared materials, imprecise targeting of nanomaterials, and inferior effect of therapy were still the serious problems to be urgently solved [13, 14]. With the aim to realize more intelligent drug loading and releasing behaviors, researchers had been continuing to develop stimulus-responsive nanomaterials, based on the idea that stimulus-responsive nanogels would undergo dissolution or conformational transformation in response to different stimuli in the environment compared to ordinary nanogels [15, 16]. For example, Manchun et al. [17] developed two types of pH-responsive nanogels, which exhibited slow release at neutral pH and significantly faster release under acidic condition. In addition, due to the complexity of external environment, multiple stimulus-responsive nanogels [18] were more effective than single stimulus-responsive nanogels in achieving accurate therapeutic effects [19–21]. If special functional units or groups were introduced into hydrogel system, it was expected to improve the biocompatibility of hydrogel, achieve the controllable release of drugs in different environments, and enrich the routes of drug delivery for nanogels [22].

✉ Hui Liu
liuhui@csu.edu.cn

[1] College of Chemistry and Chemical Engineering, Central South University, 932 South Lushan Road, Changsha, 410083 Hunan, People's Republic of China

N-isopropylacrylamide (NIPAM)-based functional hydrogels had strong stimulus responsiveness and controllable drug release, but the large-scale hydrogel carriers often encountered difficulty in penetrating into specific human tissues due to the morphology of the gel itself [23, 24]. As a kind of natural cationic alkaline polymer polysaccharide, CS, also called as deacetyl chitin, had the advantages of low price and abundant source [25–27]. If CS functional components were introduced into the NIPAM-based hydrogel system, nanoscale hydrogels could be developed by utilizing the biocompatibility advantage of natural polymer [28, 29]. The nanogels could enter human body through various drug delivery paths (e.g., oral, intravenous, etc.), and break through the biological barriers to achieve relatively deep patient site treatment as well as controlled drug releasing under different environmental conditions [30, 31].

Based on the discussion above, a nanoscale hydrogel CS/P(MAA-co-NIPAM) with both pH and temperature responsiveness was synthesized by introducing CS into the methacrylic acid (MAA) and NIPAM gel system and utilizing the intermolecular force between CS and MAA to reduce the scale of the resulting gel. The structure and scale of the gels were analyzed by various characterization means, and their stimulus response properties were also explored. Finally, the potential application possibility of drug delivery route by injection for the nanogel was investigated by the flowable property experiment, and the application in loading and controlled releasing process was studied with doxorubicin (DOX) as the model drug. Compared with the numerous literatures on hydrogels in biomedical field reported to date [32, 33], the CS/P(MAA-co-NIPAM) nanogel prepared in this work broke through the scale limitation of hydrogel-based drug carriers and made it possible to deliver drugs by injection. This nanogel with both pH and temperature responsiveness could controllably release drugs depending on the pathological environment, improve drug efficacy, and reduce drug side effects.

Experimental section

Materials

Chitosan (CS, 95% deacetylation), N-isopropylacrylamide (NIPAM, 99%), ammonium persulfate ($(NH_4)_2S_2O_8$, 98%), and acetic acid (CH_3COOH, 99%) were purchased from Adamas (China). Methacrylic acid (MAA, 99%), N,N-methylenebisacrylamide (MBA, 99%) and doxorubicin (DOX, 98%) were purchased from Aladdin (China). NIPAM and MAA were passed through a 300 mesh alkaline alumina column to remove the internally contained inhibitors, and other chemicals were used as received.

Synthesis of CS/P(MAA-co-NIPAM) nanogel by classical radical polymerization

The nanogel was prepared in acetic acid solution of CS using ammonium persulfate to initiate radical polymerization of the two monomers, and the typical procedure was as follows. Firstly, 0.5 g CS and 100 ml deionized water were added into a reaction bottle and ultrasonically dispersed for 5 min, and then 1 ml glacial acetic acid was added under magnetic stirring. Then, 2.26 g NIPAM (20 mmol) and 860 µl MAA (10 mmol) were added into the system and stirred overnight under nitrogen atmosphere. After the dissolution was completed, 60 mg MBA as the crosslinker was added to the bottle. After recharged with nitrogen, the reaction bottle was placed in an oil bath of 70 °C and magnetically stirred for 1 h. 5 ml ammonium persulfate solution (containing 57 mg ammonium persulfate) with the concentration of 0.05 mol/L was added using a syringe to initiate the polymerization reaction. Within a few minutes, the reactant mixture changed from colorless to milky white. 3 h later, the solution was centrifuged at 10,000 rpm for 40 min, followed by washing with deionized water three times to remove the residual CS and monomers. After centrifugal purification, the precipitate was freeze-dried for 36 h to obtain the targeted nanogel CS/P(MAA-co-NIPAM). The specific preparation process was shown in Fig. 1.

Samples with different monomer ratios were prepared depending on the amount of reactants used, and detailed descriptions were listed in Table 1. Unless specifically stated, the sample used in each experiment was CS/P(MAA-co-NIPAM)-3.

Characterization methods

The resulting CS/P(MAA-co-NIPAM) nanogel was characterized using Fourier transform infrared spectroscopy (Nicolet Is50) to determine corresponding characteristic functional groups. The surface element composition and chemical bonding status of CS/P(MAA-co-NIPAM) were analyzed using an X-ray photoelectron spectrometer (Escalab 250XI). The thermal stability of CS/P(MAA-co-NIPAM) was determined by a thermogravimetric analyzer (TGA-2) under nitrogen atmosphere. The crystal structure of CS/P(MAA-co-NIPAM) was examined by using an X-ray powder diffraction spectrometer (Advance D8) to analyze the physical phase and crystallinity. The microscopic morphology of CS/P(MAA-co-NIPAM) was observed by using a scanning electron microscope (Tescan Mira3).

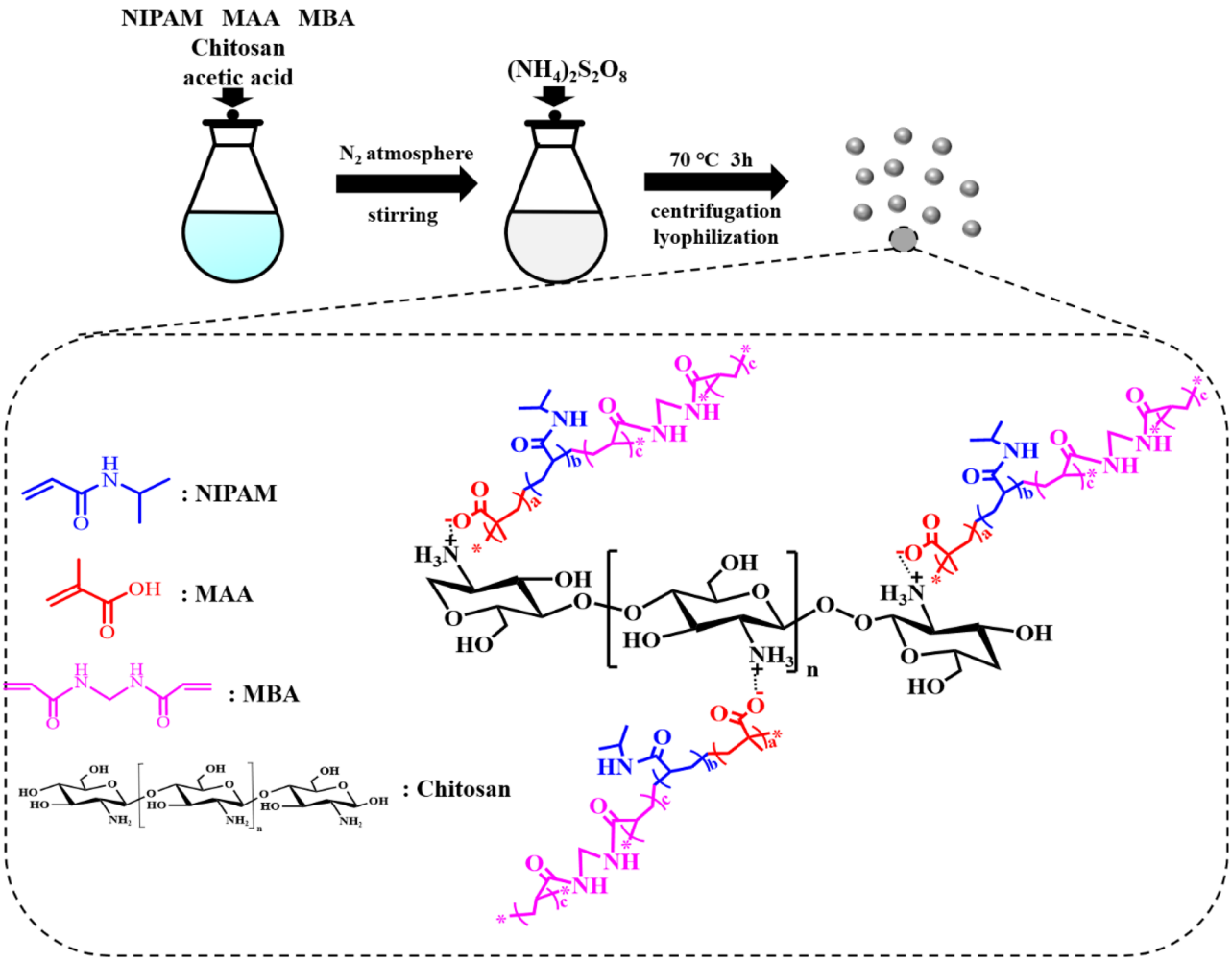

Fig. 1 Schematic diagram for the preparation of CS/P(MAA-co-NIPAM) nanogel

Stimuli-responsive performance testing

pH-responsive property experiment

The pH-responsiveness of CS/P(MAA-co-NIPAM) nanogels was indirectly reflected by the turbidity change of nanogel dispersions in different pH solutions. The typical procedure was as follows: 10 mg dry nanogel sample was ultrasonically dispersed in 15 ml aqueous solution with different pH values (pH was adjusted by using 0.1 mol/L HCl and NaOH solutions). The sample was placed in a water bath with a constant temperature oscillator at 20 °C for 12 h. The turbidity of nanogel dispersion was then measured using a turbidimeter (LH-NTU3M), and the variation curves of turbidity with pH were obtained.

Temperature-responsive property experiment

A dynamic light scattering nanoparticle size analyzer (DLS, Zetasizer Nano ZS90) was used to determine the hydration diameter of CS/P(MAA-co-NIPAM) nanogel in aqueous dispersion at different temperatures to indirectly explore their temperature responsive property. The testing procedure was as follows: 100 mg dry nanogel was dispersed and swollen in

Table 1 Specific reactant formulation for synthesis of CS/P(MAA-co-NIPAM) nanogel

Samples	CS(g)	NIPAM(mmol)	AA(mmol)	MBA(mg)	$(NH_4)_2S_2O_8$(mg)
CS/P(MAA-co-NIPAM)-1	0.5	10	6	60	57
CS/P(MAA-co-NIPAM)-2	0.5	10	10	60	57
CS/P(MAA-co-NIPAM)-3	0.5	20	10	60	57

10 ml deionized water for 12 h. The particle size distribution and hydration diameter were measured at 20 °C and 45 °C by using DLS, and the temperature-responsive performance was assessed by the change of hydration diameter.

Drug loading and releasing experiments

Drug loading performance testing

DOX was selected as a model drug to evaluate the loading capacity of the prepared samples, and the typical procedure was as follows. A certain amount of dry gel was immersed in 20 ml aqueous DOX solution with a concentration of 1 mg/ml. The mixture was placed in a water bath thermostat shaker for 24 h at constant temperature to achieve ample loading of the drug. The concentration of unloaded DOX was determined by measuring the absorbance of residual drug solution at the wavelength of 480 nm by a UV–Vis spectrophotometer (T-2600), and the drug loading efficiency (DLE) was calculated according to Eq. (1) [34].

$$\text{Drug Loading Efficiency (DLE)} = \frac{(M_T - V_1C_1)}{M_T} \times 100\% \quad (1)$$

where M_T was the total mass of initially added DOX, mg, V_1 was the volume of residual drug solution after loading, ml, and C_1 was the concentration of DOX in residual drug solution after loading, mg/ml.

In-vitro drug controlled releasing behaviors testing

According to the result of drug loading testing, the most suitable sample was selected to test its in-vitro drug controlled releasing behaviors under different environmental stimulation conditions. The procedure was as follows: a certain mass of drug-loaded gel was put into the media under different environmental conditions (pH was adjusted by HCl solution and PBS solution, and temperature was controlled as 20 °C and 45 °C). The initial volume of control solution was 20 ml, and 2 ml supernatant was taken out at certain time interval. The absorbance of the supernatant at the wavelength of 480 nm was measured by UV–Vis spectrophotometer, and then the supernatant was poured back to the original mixture to keep the constant volume. The concentration of DOX was determined according to the absorbance, and the release efficiency (RE) of nanogel toward DOX was calculated according to Eq. (2) [35].

$$\text{Release Efficiency (RE)} = \frac{V_0C_t}{M_0} \times 100\% \quad (2)$$

where M_0 was the total mass of the initial DOX in the nanogel, mg, V_0 was the volume of dissolved medium, ml, and C_t was the concentration of DOX in dissolved medium at time t, mg/ml.

Results and discussion

Structure confirmation of the nanogel

Internal molecular structure analysis of the nanogel (FT-IR)

In order to clarify the specific molecular structure of the nanogel, CS and the synthesized CS/P(MAA-co-NIPAM) nanogel were subjected to FT-IR characterization testing, and the results were shown in Fig. 2a. As could be observed, several new characteristic absorption peaks appeared in the curve of CS/P(MAA-co-NIPAM) (Fig. 2a-ii) compared to CS (Fig. 2a-i). For example, the characteristic peaks of O–H and C = O stretching vibrations in carboxyl groups were found at 3200–2800 cm^{-1} and 1710 cm^{-1}, [36] respectively, indicating the existence of MAA unit in the nanogel. The characteristic peaks of C-H distorted vibrations in isopropyl (-$CH(CH_3)_2$) appeared at 1388 cm^{-1} and 1368 cm^{-1}, [37] meaning the presence of NIPAM unit. The absorption peaks at 1648 cm^{-1} and 1543 cm^{-1} could be assigned to C = O stretching vibration and N–H distorted vibration in acylamine group (-CO–NH-) [38], respectively. The absorption peak of -CH_2- distorted vibration at 1460 cm^{-1} could verify the presence of MBA unit in the nanogel. Notably, the absorption peak of the C–O–C stretching vibration was shifted from 1149 cm^{-1} to 1171 cm^{-1}, which was possibly owing to the interaction between CS and the copolymer [39]. In summary, FT-IR result tentatively confirmed the successful synthesis of CS/P(MAA-co-NIPAM) nanogel.

Surface elemental composition analysis of the nanogel (XPS)

X-ray photoelectron spectroscopy (XPS) was used to analyze the surface elemental content and binding status of CS and CS/P(MAA-co-NIPAM). The survey XPS curves were demonstrated in Fig. 2b, and the surface elemental composition was listed in Table 2. It was clearly seen that the relative content of carbon and nitrogen elements on the surface of CS/P(MAA-co-NIPAM) increased compared to that of CS, while the relative content of oxygen element decreased to a larger extent [40]. The result could be attributed to the encapsulation of CS segments by the polymeric network with long carbon chains after polymerization. Based on the above results, it might be reasonably speculated that CS/P(MAA-co-NIPAM) nanogels had been successfully synthesized by radical polymerization.

To further determine the molecular structure of CS/P(MAA-co-NIPAM) nanogel, the characteristic peaks of C1s, O1s, and N1s in the XPS survey spectra of CS and

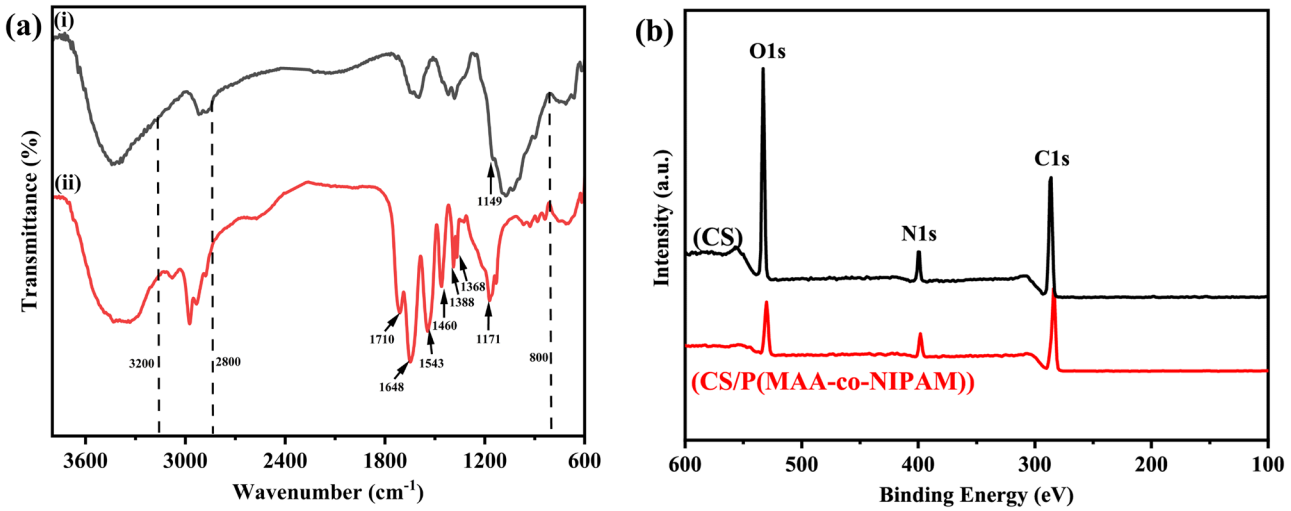

Fig. 2 **a** FT-IR absorption spectra of (i) CS and (ii) CS/P(MAA-co-NIPAM) nanogel; **b** XPS survey spectra of CS and CS/P(MAA-co-NIPAM) nanogel

CS/P(MAA-co-NIPAM) were split-peak fitted, and the results were displayed in Fig. 3. As could be seen from the split-peak fitting curves of C1s in Fig. 3a and b, the C1s of the nanogel changed from a single peak to a duplex peak, and all the binding energies of five bonds decreased after the polymerization, which might be attributed to the formation of interactive force during the polymerization. Furthermore, compared to those of CS, the fitting peak intensities of C–C and C = O bonds of CS/P(MAA-co-NIPAM) were significantly increased, and the fitting peak intensities of C–OH and C–O–C bonds of the nanogel were markedly decreased.

As a comparison of O1s fitting for CS in Fig. 3c, a new fitting peak corresponding to carboxyl group was observed in the split-peak fitting curve of O1s for CS/P(MAA-co-NIPAM) in Fig. 3d. Moreover, dramatic increase in fitting peak of acylamine group and obvious decrease in fitting peak of C–OH also proved the possible interaction between the polymeric layer and CS unit.

According to the fitting curves of N1s in Fig. 3e and Fig. 3f, the fitting peak intensity of C-NH_2 decreased and peak intensity of acylamine group increased. Compared to that in CS, the binding energy of acylamine group in the nanogel was obviously shifted to a low position. From XPS results, it was also concluded that CS/P(MAA-co-NIPAM) nanogels had been successfully synthesized.

Table 2 Results of XPS analysis on surface elemental composition of CS and CS/P(MAA-co-NIPAM) nanogel

Samples	C (atomic%)	O (atomic%)	N (atomic%)
CS	60.29	31.97	7.74
CS/P(MAA-co-NIPAM)	73.93	16.45	9.62

Thermal stability analysis of the nanogel (TGA)

Thermogravimetric analysis (TGA) testing was performed on the CS/P(MAA-co-NIPAM) nanogel sample to analyze its thermal stability, and the result was shown in Fig. 4a. From the thermogravimetric curve, it could be seen that the weight loss process of CS/P(MAA-co-NIPAM) could be divided into three stages. The first stage was from room temperature to about 105 °C with a weight loss of 10.2%, and the weight loss at this stage was caused by the evaporation of free water remaining in the nanogel. The second stage was from 105 °C to around 360 °C with a weight loss of 21.4%, and the reason was that the continuous increase of temperature led to the deep volatilization of internal binding water inside the nanogel. The total weight loss (68.4%) of the third stage from 360 °C to 800 °C could be attributed to thermal decomposition of both organic backbone and CS chain segments. It was suggested that CS/P(MAA-co-NIPAM) nanogel could effectively maintain its structural stability in the temperature range of the physiological environment, and be potentially applied in the biomedical field.

Crystallinity analysis of the nanogel (XRD)

XRD was employed to analyze the crystallinity difference of CS and CS/P(MAA-co-NIPAM), and the result was demonstrated in Fig. 4b. The curve of CS showed that two characteristic peaks appeared at $2\theta = 12°$ and 20.1°, owing to two crystalline states of CS, hydrated crystalline and anhydrous crystalline, respectively [41]. In contrast, in the pattern of CS/P(MAA-co-NIPAM), the characteristic peak at $2\theta = 12°$ had disappeared and the diffraction peak originally at $2\theta = 20.1°$ had been shifted to low diffraction angle. This

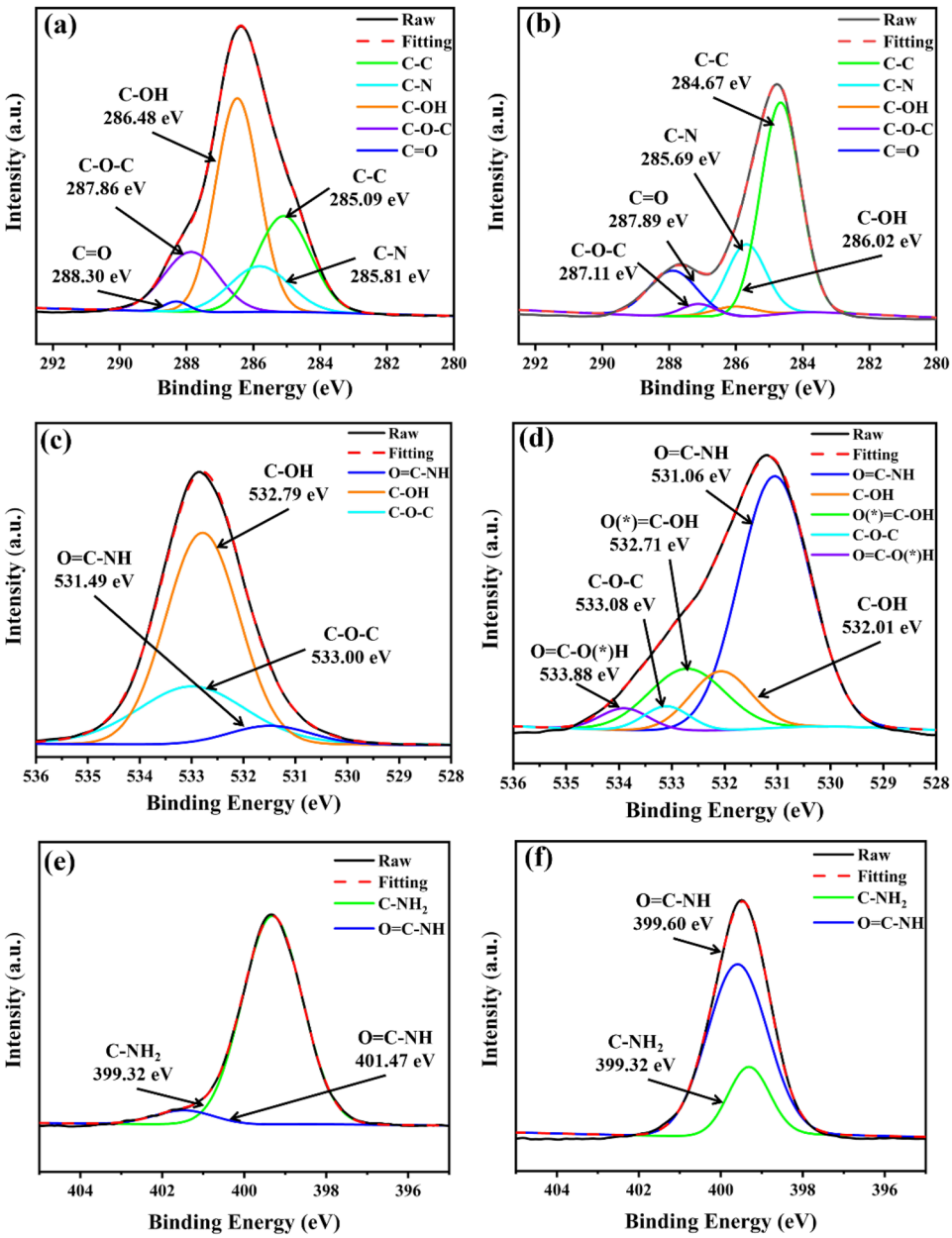

Fig. 3 XPS split-peak fitting plots: **a** C1s, **c** O1s, and **e** N1s fitting curves of CS; **b** C1s, **d** O1s, and **f** N1s fitting curves of CS/P(MAA-co-NIPAM)

result indicated that strong interaction took place between the polymer and CS during the synthetic process, which led to a certain degree of decrease in crystallinity of the resulting nanogel.

Surface morphology analysis of the nanogels (SEM)

The morphology of nanogels was observed by scanning electron microscopy (SEM), and the results were presented in Fig. 4c. It could be seen from Fig. 4c-i that CS/P(MAA-co-NIPAM)-1 exhibited relatively regular spherical morphology with the diameter slightly less than 100 nm, and the particles were stacked with each other and adhered closely. As could be observed in Fig. 4c-ii, CS/P(MAA-co-NIPAM)-2 also showed a spherical shape with a particle size around 100 nm, but the nanogel was more granular than CS/P(MAA-co-NIPAM)-1. In Fig. 4c-iii, CS/P(MAA-co-NIPAM)-3 exhibited a regular block shape with uniform particle size, and the particle size of particles was slightly larger than 100 nm as clearly displayed in the partial enlargement as demonstrated in Fig. 4c-iv. On one hand, as the amount of MAA monomer increased, the enhancement of electrostatic repulsion between CS and hydrogel network made gel particles move more freely, leading to the improvement of the dispersibility. On the other hand, with the increasing usage of NIPAM monomer,

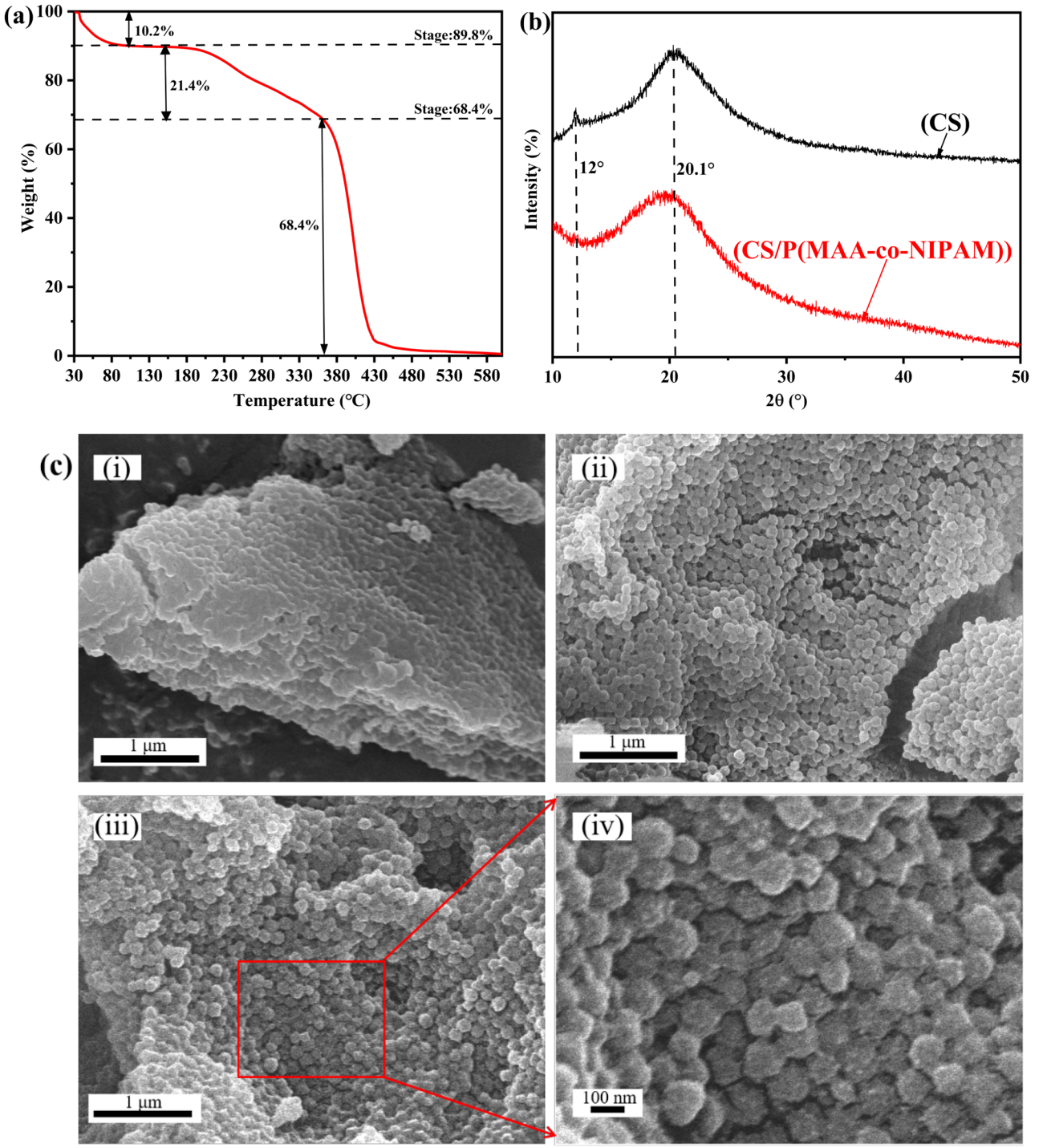

Fig. 4 **a** Thermogravimetric curve of CS/P(MAA-co-NIPAM) nanogel; **b** XRD patterns of CS and CS/P(MAA-co-NIPAM) nanogel; **c** SEM images of (i) CS/P(MAA-co-NIPAM)-1, (ii) CS/P(MAA-co-NIPAM)-2, (iii) CS/P(MAA-co-NIPAM)-3, and (iv) partial enlargement of CS/P(MAA-co-NIPAM)-3

the hydrophobic isopropyl content in the hydrogel network was also increased correspondingly, and the subsequent hydrophobic effect gave rise to even distribution of internal water in the nanogel during the synthetic process, which endowed the finally prepared nanogel with relatively regular morphology.

Stimuli-responsive properties of the nanogels

pH-responsive property analysis

The pH-responsiveness of the samples was indirectly assessed by the turbidity change in aqueous dispersions with different pH values. The testing results of turbidity at different pH conditions and the appearance change of the aqueous dispersion were shown in Fig. 5a and c, respectively. It could be seen from Fig. 5a that the turbidity of aqueous dispersion of the nanogel in acidic environment was significantly higher than that in neutral and alkaline environments, which was consistent with the appearance change observed from Fig. 5c. Due to the protonation of carboxyl groups in MAA unit and amine groups in CS unit of the nanogel under acidic condition, the whole polymeric network shrunk hydrophobically and the overall particle size decreased, leading to poor hydrophilicity of the nanogel. And then the nanogel "precipitated" from the solution on a macroscopic scale, resulting in a high turbidity of the aqueous dispersion. Under the alkaline condition, influenced by the repulsive force of OH- in the solution, the whole polymer network underwent swelling and expansion, leading to a good dispersion of the nanogel in solution and a decrease in turbidity. pH-responsive testing results showed that CS/P(MAA-co-NIPAM) had an obvious pH-responsive property.

Temperature-responsive property analysis

Dynamic light scattering (DLS) testing was performed on the aqueous dispersion of CS/P(MAA-co-NIPAM) nanogel, and the result was demonstrated in Fig. 5b. It was obvious from Fig. 5b that hydration diameter (D_h) of the nanogel at 45 °C (145 nm) was smaller compared with that at 20 °C (234 nm). Meanwhile, the polydispersity indexes of particle size at 20 °C and 45 °C were calculated as 0.056 and 0.075, respectively, indicating that the prepared nanogel had uniform size and narrow particle size distribution. It should be noted that the hydration diameter obtained from DLS was larger than the size of dry gel particles observed in SEM

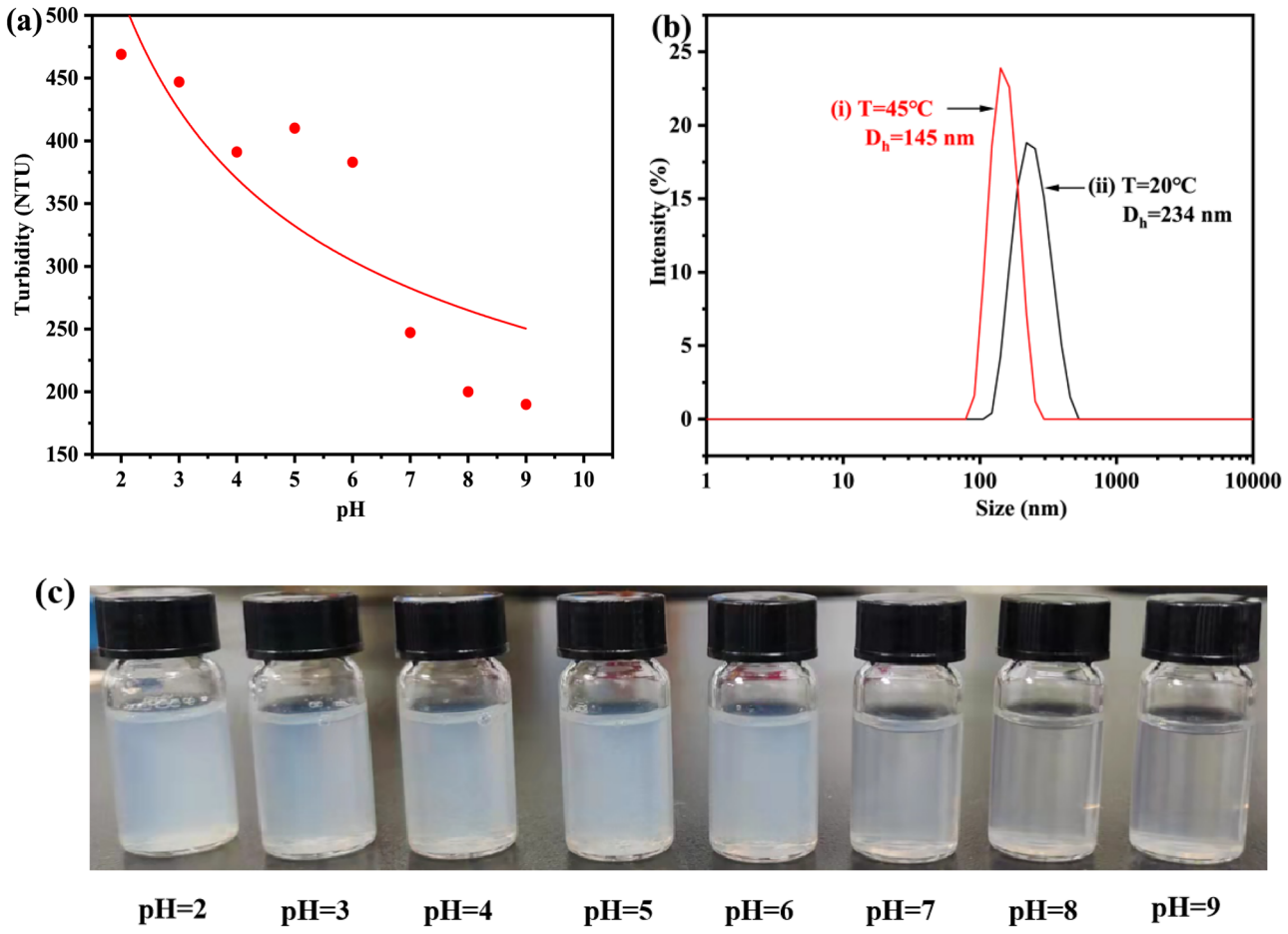

Fig. 5 **a** Turbidity of CS/P(MAA-co-NIPAM) nanogel in aqueous dispersion at different pHs, **b** DLS analysis result of CS/P(MAA-co-NIPAM) nanogel at (i) 45 °C and (ii) 20 °C, and **c** the appearance of CS/P(MAA-co-NIPAM) nanogel in aqueous dispersions with different pHs

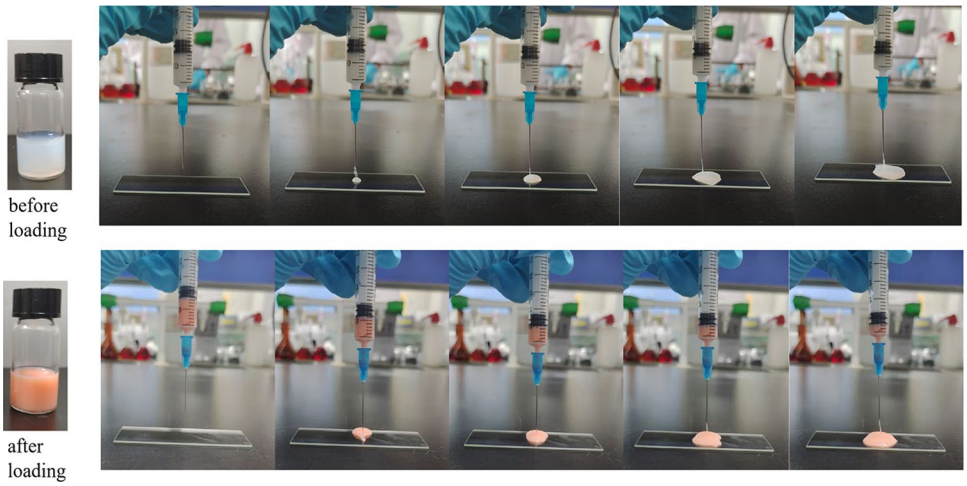

Fig. 6 Schematic diagram of CS/P(MAA-co-NIPAM) nanogel used in simulative drug delivery by injection

(Fig. 4c). The reason was that the nanogel would undergo swelling in aqueous dispersion and absorb water to make the particle size larger. Therefore, it could be concluded that CS/P(MAA-co-NIPAM) nanogel had strong temperature-responsive performance.

Exploring the drug delivery route of CS/P(MAA-co-NIPAM) nanogel

CS/P(MAA-co-NIPAM) nanogel had the potential to be administered by injection in addition to the oral route due to its nanoscale advantage. As shown in Fig. 6, the nanogel dispersion before and after drug loading could be smoothly extruded by using a simple syringe, and the injected hydrogel could spread out automatically, which was an advantageous flowable feature not possessed by large-scale gel carriers. Therefore, CS/P(MAA-co-NIPAM) nanogel was expected to achieve the drug delivery process by intravenous injection, thus expanding application domain and targeting performance of the gel carriers.

Drug loading and in-vitro controlled releasing

Loading of model drug

The drug loading efficiencies of the three nanogel samples with different monomer ratios were shown in Table 3. As could be seen, the CS/P(MAA-co-NIPAM)-2 and CS/P(MAA-co-NIPAM)-3 samples with higher amount of MAA unit exhibited higher loading efficiency for DOX than CS/P(MAA-co-NIPAM)-1. The difference might be explained by the viewpoint that the drug loading process of CS/P(MAA-co-NIPAM) toward DOX was intrinsically driven by the electrostatic interaction between negatively charged carboxyl groups in MAA unit and positively charged DOX molecules. Meanwhile, the higher MAA content, the higher drug loading efficiency for DOX molecules. From previous SEM characterization results in Fig. 4c, it could be seen that the increase of MAA content was beneficial to the enhancement of dispersion degree for nanogel particles. Thus, the contact area between the independent gel particles and DOX molecules was expanded, and the drug loading efficiency was further increased. Therefore, the CS/P(MAA-co-NIPAM)-3 sample with the highest drug loading efficiency was selected for the subsequent in-vitro controlled releasing experiments.

Table 3 Comparison of drug loading efficiency in different CS/P(MAA-co-NIPAM) nanogel samples

Samples	Loaded drug (mg)	Drug Loading Efficiency (%)
CS/P(MAA-co-NIPAM)-1	8.35	41.75
CS/P(MAA-co-NIPAM)-2	16.38	81.90
CS/P(MAA-co-NIPAM)-3	16.80	84.00

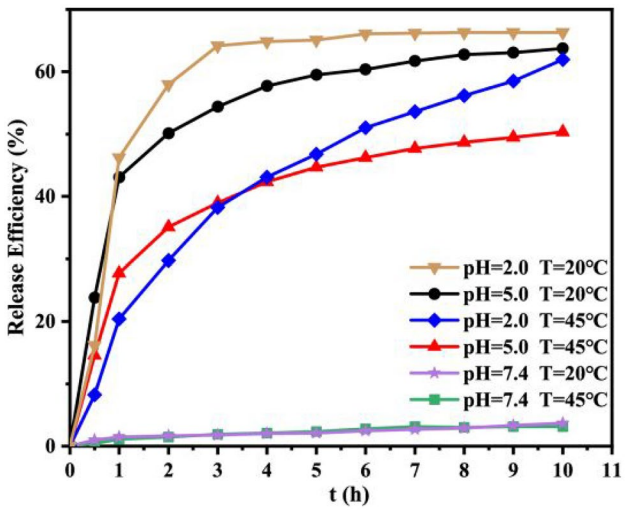

Fig. 7 Release profiles of CS/P(MAA-co-NIPAM) nanogel with DOX as the model drug under different stimulation conditions

Table 4 Original and rewritten formula of the drug releasing kinetic models

Kinetic Models	Original Formula	Rewritten Formula
Zero order	$F = k_0 t$	$F = k_0 t$
First order	$F = 1 - e^{-k_1 t}$	$-\ln(1-F) = k_1 t$
Higuchi	$F = k_H t^{0.5}$	$F = k_H t^{0.5}$
Korsmeyer-Peppas	$F = k_{KP} t^n$	$lgF = nlgt + lgk_{KP}$

In-vitro controlled releasing behavior of model drug

The in-vitro drug releasing profiles of CS/P(MAA-co-NIPAM) hydrogel loaded with the model drug DOX at different temperatures and pH conditions were shown in Fig. 7. As could be seen, the final drug release efficiency was very low at pH = 7.4 regardless of the solution temperature, indicating that temperature change had no obvious effect on release efficiency of the nanogel. When pH was 5.0, the ultimate release efficiency at 20 °C reached 63.73%, which was higher than that at 45 °C (RE = 50.36%). At the same temperature, the release efficiency at pH = 5.0 was slightly higher than that at pH = 2.0 at the beginning of drug releasing process, but the final equilibrium release efficiency was lower than that at pH = 2.0. The possible reason for this phenomenon was related to molecular conformation of the nanogel and the drug delivery mechanism. For CS/P(MAA-co-NIPAM) nanogel, both pH and temperature would affect the drug releasing process mainly by changing overall conformation of the nanogel, while temperature change might also alter the hydrophilic and hydrophobic equilibrium of polymeric network in the nanogel. Moreover, the highest drug release efficiency of 66.30% was observed at pH = 2.0 & T = 20 °C. In summary, the drug releasing behaviors of

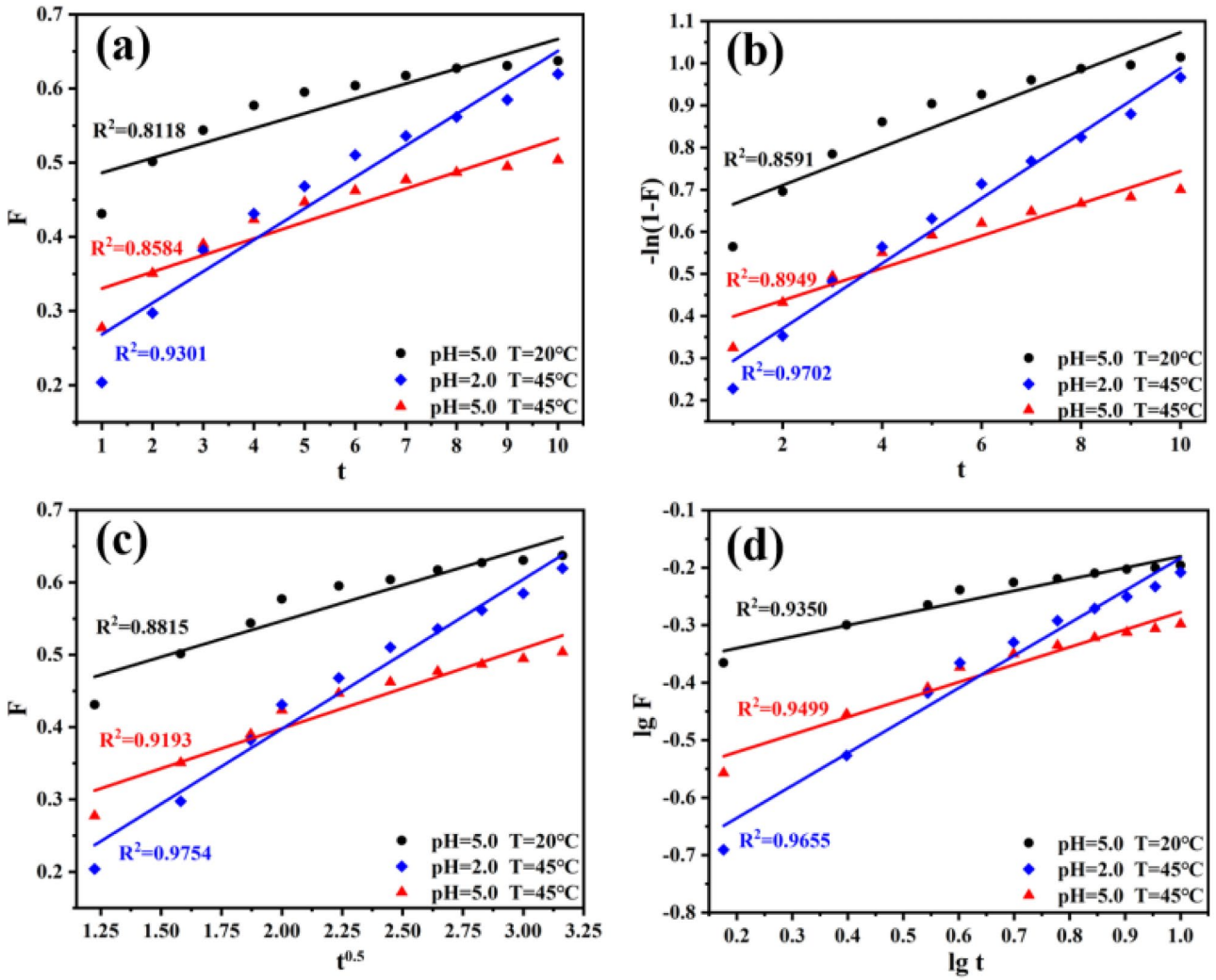

Fig. 8 Results of fitting pharmacokinetic models for the drug releasing behaviors of CS/P(MAA-co-NIPAM) with **a** zero-level kinetic model, **b** first-level kinetic model, **c** Higuchi model, and **d** Korsmeyer-Peppas model

the nanogel could be accurately controlled by adjusting pH and temperature conditions of the environment to achieve the controllable drug delivery in physiological environment.

Kinetic model fitting of drug releasing

Four kinetic models (Zero order, First order, Higuchi, and Korsmeyer-Peppas models) were used to mimic the releasing behaviors of CS/P(MAA-co-NIPAM) toward DOX under different conditions from the data level. The original and rewritten formulas of the four models were listed in Table 4, and the final fitting straight lines were shown in Fig. 8. Besides, the corresponding R^2 was labeled next to the corresponding straight lines.

Comparison of R^2 values in the fitting result indicated that Korsmeyer-Peppas model was the most suitable for describing the releasing behaviors of DOX at pH = 5.0 & T = 20 °C and pH = 5.0 & T = 45 °C. And Higuchi model was better fitted for the drug releasing process at pH = 2.0 & T = 45 °C. From the perspective of stimuli-responsive properties, CS/P(MAA-co-NIPAM) nanogel existed in aqueous dispersion mainly in the form of independent gel particles after sufficient dissolution. CS/P(MAA-co-NIPAM) nanogel could be approximately regarded as drug-loaded hydrogel microspheres dispersed in dissolution medium. The fitting results contributed to a deep understanding of the drug releasing behaviors of CS/P(MAA-co-NIPAM) nanogel. It could be concluded from the data level that environmental stimulation conditions not only changed the drug release efficiency of CS/P(MAA-co-NIPAM) nanogel, but also exerted an effect on the drug releasing pattern of the nanogel.

Mechanism analysis of drug delivery

Through the characterization results of CS/P(MAA-co-NIPAM) nanogel and the analysis of drug loading and releasing behaviors, schematic diagram of responsive behaviors, chemical structure of the nanogel, and the loading and releasing mechanism was demonstrated in Fig. 9. The nanogel could be considered as a three-dimensional structure with polymeric network as the shell and CS chain segments as the core. The interaction inside the shell-core structure rendered the independent gel particles to present a morphological feature similar to a sphere. After the nanogel was dispersed in DOX solution, the positively charged DOX molecules entered the interior of the nanogel together with moisture, and then DOX molecules were combined with the negatively charged carboxyl groups through electrostatic interaction to complete the loading process. Finally, under the stimulation of external environmental temperature and pH changes, the nanogel underwent different degrees of shrinking and swelling behaviors. The internally loaded DOX molecules were released to the outside of the gel system by molecular diffusion under the influence of environment stimulus to realize the drug releasing process.

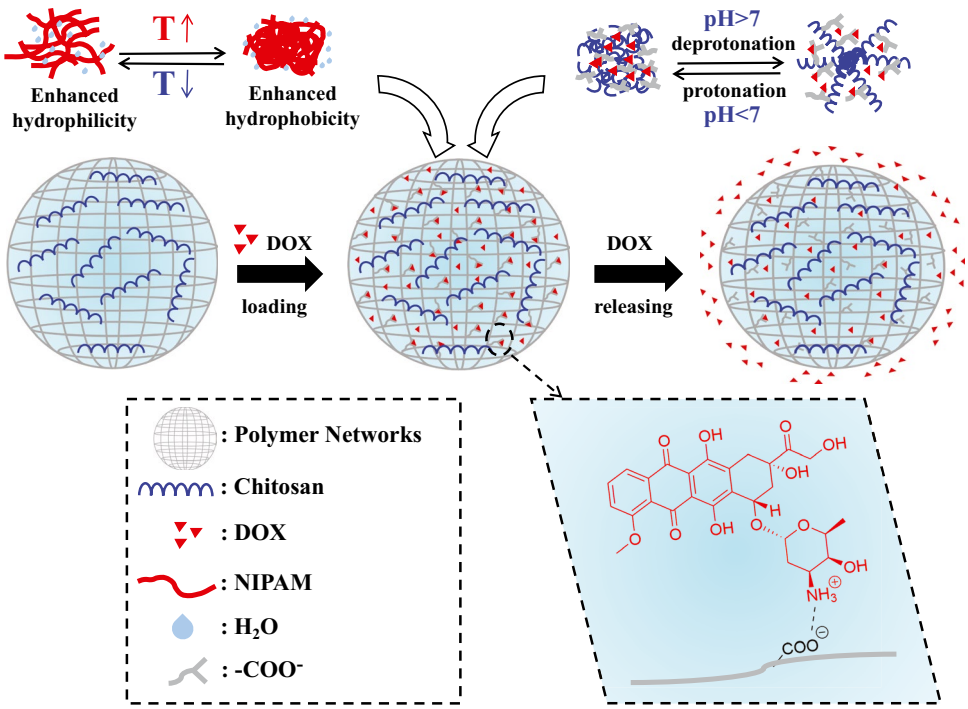

Fig. 9 Schematic diagram of responsive behaviors, chemical structure of the nanogel, and the loading and releasing mechanism for DOX

Conclusion

In summary, CS-functionalized pH and temperature dual-responsive nanogel CS/P(MAA-co-NIPAM) was prepared by classical radical polymerization and applied in the loading and releasing process of DOX. The molecular structure and elemental composition of CS/P(MAA-co-NIPAM) were determined by FT-IR and XPS. It was found that the nanogel had strong thermal stability by TGA testing, and the dry gel particle size was observed to be around 100 nm by SEM. CS/P(MAA-co-NIPAM) was proved to possess obvious pH and temperature responsive properties. The D_h of CS/P(MAA-co-NIPAM) in aqueous dispersion was 234 nm at 20 °C and 154 nm at 45 °C, respectively. The schematic flowable characteristic by injection experiment indicated that the nanogel possessed the possibility of drug delivery by injection. Drug loading efficiency of CS/P(MAA-co-NIPAM)-3 sample could attain 84.00%, and the release efficiency of the nanogel was the highest at pH = 2.0 & T = 20 °C. It was suggested that changes in environmental conditions would not only affect the overall structure and drug release efficiency of the nanogel, but also cause the change in drug releasing pattern. Finally, the drug loading and releasing mechanism of the nanogel was analyzed, and it was found that DOX molecules were loaded into the nanogel network through electrostatic interactions, and releasing driving force of the drug from the gel was owing to molecular diffusion. Based on this, CS/P(MAA-co-NIPAM) nanogel was expected to achieve controllable release of loaded drugs under different physiological environments, which might provide promising application prospects in angiography, tissue repair, and cellular therapy.

Acknowledgements This work was financially supported by Natural Science Foundation of Hunan Province (2022JJ30683) and Natural Science Foundation of Changsha City (kq2202086). The authors would like to thank Shiyanjia Lab (www.shiyanjia.com) for XRD and TGA analysis. Hui Liu also thanked for the kind technical help from Advanced Research Center of Central South University, China, especially in the testing of SEM and XPS.

Author contributions Danyang Li: Investigation, Data curation, Writing – original draft. Wenshuang Xu: Investigation, Data curation, Writing – review & editing. Hui Liu: Supervision, Project administration, Writing – review & editing.

Data availability Data will be made available on request.

Declarations

Competing interest The authors declare that they have no known competing financial interests or personal relationships that could have appeared to influence the work reported in this paper.

References

1. Zhang H-F, Ma L, Su F, Ma X-F, Li T, Jian-Zha-Xi W, Zhao G-H, Wu Z-M, Hou C-L, Yan H-J (2021) Ph and reduction dual-responsive feather keratin - sodium alginate nanogels with high drug loading capacity for tumor-targeting dox delivery. Polym Test 103:107375
2. Preman NK, Barki RR, Vijayan A, Sanjeeva SG, Johnson RP (2020) Recent developments in stimuli-responsive polymer nanogels for drug delivery and diagnostics: A review. Eur J Pharm Biopharm 157:121–153
3. Zhao Y, Cao W, Liu Y (2020) Recent advances in polymeric nano-sized carrier systems. Chem J Chinese U 41(5):909–923
4. Salem AK, Lu X (2021) National institute for pharmaceutical technology & education (nipte) research and perspective: Advances in nanotechnology-based drug delivery. AAPS PharmSciTech 22(4):152
5. Dong Y, Li S, Li X, Wang X (2021) Smart mxene/agarose hydrogel with photothermal property for controlled drug release. Int J Biol Macromol 190:693–699
6. Wang X, Li C, Wang Y, Chen H, Zhang X, Luo C, Zhou W, Li L, Teng L, Yu H, Wang J (2022) Smart drug delivery systems for precise cancer therapy. Acta Pharm Sin B 12(11):4098–4121
7. Oh Y, Kim S-H (2022) Hydrogel-shelled biodegradable microspheres for sustained release of encapsulants. J Polym Sci 60(11):1700–1709
8. Quazi MZ, Park N (2022) Nanohydrogels: Advanced polymeric nanomaterials in the era of nanotechnology for robust functionalization and cumulative applications. Int J Mol Sci 23(4):1–19
9. Wei Z, Lin Q, Yang J, Long S, Zhang G, Wang X (2020) Fabrication of novel dual thermo- and ph-sensitive poly (n-isopropylacrylamide-n-methylolacrylamide-acrylic acid) electrospun ultrafine fibres for controlled drug release. Mater Sci Eng C 115:111050
10. Maddiboyina B, Desu PK, Vasam M, Challa VT, Surendra AV, Rao RS, Alagarsamy S, Jhawat V (2022) An insight of nanogels as novel drug delivery system with potential hybrid nanogel applications. J Biomat Sci-Poym E 33(2):262–278
11. Azadi A, Hamidi M, Rouini MR (2013) Methotrexate-loaded chitosan nanogels as "trojan horses" for drug delivery to brain: Preparation and in vitro/in vivo characterization. Int J Biol Macromol 62:523–530
12. Rudmianeh HR, Shourian M, Ansari R, Pirbasti FG, Asghari SM (2021) Polysaccharide nanogels for the delivery of gemcitabine hydrochloride. Acs Appl Polym Mater 3(12):6345–6358
13. Baby T, Liu Y, Yang G, Chen D, Zhao C-X (2021) Microfluidic synthesis of curcumin loaded polymer nanoparticles with tunable drug loading and ph-triggered release. J Colloid Interf Sci 594:474–484
14. Ozkan SA, Dedeoglu A, Karadas Bakirhan N, Ozkan Y (2019) Nanocarriers used most in drug delivery and drug release: Nanohydrogel, chitosan, graphene, and solid lipid'. Turk J Pharm Sci 16(4):481–492
15. Nikolova D, Ruseva K, Tzachev C, Christov L, Vassileva E (2022) Novel poly(sulfobetaine methacrylate) based carriers as potential ocular drug delivery systems for timolol maleate. Polym Int 71(6):662–667
16. Pourkhatoun M, Kalantari M, Kamyabi A, Moradi A (2022) Preparation and characterization of ph-sensitive carboxymethyl cellulose-based hydrogels for controlled drug delivery. Polym Int 71(8):991–998

17. Manchun S, Dass CR, Cheewatanakornkool K, Sriamornsak P (2015) Enhanced anti-tumor effect of ph-responsive dextrin nanogels delivering doxorubicin on colorectal cancer. Carbohydr Polym 126:222–230
18. Chen Z, Liao T, Wan L, Kuang Y, Liu C, Duan J, Xu X, Xu Z, Jiang B, Li C (2021) Erratum to: Dual-stimuli responsive near-infrared emissive carbon dots/hollow mesoporous silica-based integrated theranostics platform for real-time visualized drug delivery. Nano Res 14(11):4365–4365
19. Van Gheluwe L, Chourpa I, Gaigne C, Munnier E (2021) Polymer-based smart drug delivery systems for skin application and demonstration of stimuli-responsiveness. Polymers (Basel) 13(8):1–31
20. Serrano-Medina A, Oroz-Parra I, Gomez-Resendiz VE, Licea-Navarro AF, Licea-Claveríe Á, Cornejo-Bravo JM (2018) Temperature- and ph-sensitive core–shell nanogels as efficient carriers of doxorubicin with potential application in lung cancer treatment. Int J Polym Mater 67:20–26
21. Qin G, Hu C, Jiang Y, Dong S, Liu L, Zhao H (2021) Ph/enzyme/light triple-responsive vesicles from lysine-based amphiphilic diblock copolymers. J Polym Sci 59(17):1958–1971
22. Bardajee GR, Hooshyar Z (2018) Thermo/ph/magnetic-triple sensitive poly(n-isopropylacrylamide-co-2-dimethylaminoethyl) methacrylate)/sodium alginate modified magnetic graphene oxide nanogel for anticancer drug delivery. Polym Bull 75(12):5403–5419
23. Xu X, Liu Y, Fu W, Yao M, Ding Z, Xuan J, Li D, Wang S, Xia Y, Cao M (2020) Poly(n-isopropylacrylamide)-based thermoresponsive composite hydrogels for biomedical applications. Polymers (Basel) 12(3):1–22
24. Feng S, Wang S, Lv Y, He L, Li Q, Zhang T (2019) Dual ph- and thermal-responsive nanocomposite hydrogels for controllable delivery of hydrophobic drug baicalein. Polym Int 68(3):494–502
25. Wen Y, Li F, Li C, Yin Y, Li J (2017) High mechanical strength chitosan-based hydrogels cross-linked with poly(ethylene glycol)/polycaprolactone micelles for the controlled release of drugs/growth factors. J Mater Chem B 5(5):961–971
26. McCarthy PC, Zhang Y, Abebe F (2021) Recent applications of dual-stimuli responsive chitosan hydrogel nanocomposites as drug delivery tools. Molecules 26(16):1–15
27. Murugesan S, Scheibel T (2021) Chitosan-based nanocomposites for medical applications. J Polym Sci 59(15):1610–1642
28. Xu Y, Li Y, Chen Q, Fu L, Tao L, Wei Y (2018) Injectable and self-healing chitosan hydrogel based on imine bonds: Design and therapeutic applications. Int J Mol Sci 19(8):1–16
29. Shao D, Gao Q, Sheng Y, Li S, Kong Y (2022) Construction of a dual-responsive dual-drug delivery platform based on the hybrids of mesoporous silica, sodium hyaluronate, chitosan and oxidized sodium carboxymethyl cellulose. Int J Biol Macromol 202:37–45
30. Gao Y, Li Z, Huang J, Zhao M, Wu J (2020) In situ formation of injectable hydrogels for chronic wound healing. J Mater Chem B 8(38):8768–8780
31. Kang SX, He YY, Yu DG, Li WB, Wang K (2021) Drug-zein@lipid hybrid nanoparticles: Electrospraying preparation and drug extended release application. Colloid Surface B 201:1–8
32. Yang F, Wang J, Song S, Rao P, Wang R, Liu S, Xu L, Zhang F (2020) Novel controlled release microspheric soil conditioner based on the temperature and ph dual-stimuli response. J Agric Food Chem 68(30):7819–7829
33. Md Rasib SZ, Md Akil H, Khan A, Abdul Hamid ZA (2019) Controlled release studies through chitosan-based hydrogel synthesized at different polymerization stages. Int J Biol Macromol 128:531–536
34. Gan Q, Wang T (2007) Chitosan nanoparticle as protein delivery carrier–systematic examination of fabrication conditions for efficient loading and release. Colloids Surf B Biointerfaces 59(1):24–34
35. Lin X, Ju X, Xie R, Jiang M, Wei J, Chu L (2013) Halloysite nanotube composited thermo-responsive hydrogel system for controlled-release. Chinese J Chem Eng 21(9):991–998
36. Chen H, Wang W, Li G, Li C, Zhang Y (2011) Synthesis of p(st-maa)-fe3o4/ppy core–shell composite microspheres with conductivity and superparamagnetic behaviors. Synth Met 161(17):1921–1927
37. Shao L, Cao Y, Li Z, Hu W, Li S, Lu L (2018) Dual responsive aerogel made from thermo/ph sensitive graft copolymer alginate-g-p(nipam-co-nhmam) for drug controlled release. Int J Biol Macromol 114:1338–1344
38. Zheng D, Wang K, Bai B, Hu N, Wang H (2022) Swelling and glyphosate-controlled release behavior of multi-responsive alginate-g-p(nipam-co-ndeam)-based hydrogel. Carbohyd Polym 282:119113
39. Kumirska J, Czerwicka M, Kaczyński Z, Bychowska A, Brzozowski K, Thöming J, Stepnowski P (2010) Application of spectroscopic methods for structural analysis of chitin and chitosan. Mar Drugs 8(5):1567–1636
40. Mathew ZP, Shamnamol GK, Greeshma KP, John S (2023) Insight on the corrosion inhibition of nanocomposite chitosan/boron nitride integrated epoxy coating system against mild steel. Corrosion Communications 9:36–43
41. Samuels RJ (1981) Solid state characterization of the structure of chitosan films. J Polym Sci B Polym Phys 19(7):1081–1105